Crystallization in Fe- and Co-Based Amorphous Alloys Studied by *In-Situ* X-Ray Diffraction

L.J. ZHANG, P.F. YU, H. CHENG, M.D. ZHANG, D.J. LIU, Z. ZHOU, Q. JIN, P.K. LIAW, G. LI, and R.P. LIU

The amorphous alloys, $Fe_{80}Si_{20}$, $Fe_{78}Si_9B_{13}$, and $Fe_4Co_{67}Mo_{1.5}Si_{16.5}B_{11}$, were prepared by the spinning method in pure argon. The crystallization behaviors of the three amorphous alloys were researched by *in-situ* X-ray diffraction (XRD), and the crystallization activation energy was calculated, based on the results of differential scanning calorimetry. The crystallization mechanism of the Fe- and Co-based alloys was analyzed, based on the experimental data. The transformation kinetics was described in terms of Johnson–Mehl–Avrami kinetics, except that the Avrami exponent of the $Fe_{78}Si_9B_{13}$ amorphous alloy annealed at 753 K (480 °C) was 4.12; the obtained values for the overall Avrami exponents of the other three amorphous alloys were below 1, as usually found for the Fe-Si amorphous alloys.

DOI: 10.1007/s11661-016-3761-7
© The Minerals, Metals & Materials Society and ASM International 2016

I. INTRODUCTION

THE Fe- and Co-based amorphous alloys have attracted great attention because of their high glass-forming ability and good mechanical and magnetic properties.[1] In a weak magnetic field, they all have a speedy response and high stabilization[2] and can be used in electrodynamic potential generators to reduce jitter due to large Barkhausen and Matteucci effects.[3] The Fe- and Co-based amorphous alloys exhibit good soft magnetic properties.[1,4] For example, Fe-based amorphous alloys with high saturation magnetization up to 1.7 T, low coercive force of 3.3 to 6.2 A/m, and high effective permeability of 8300 to 15,000 were synthesized in the Fe-B-Si-P alloy system.[5] The upper strength limit of glassy alloys was significantly increased to over 4000 MPa for Fe- and Co-based bulk glassy alloys, which can be used as a new type of ultrahigh strength material.[6] With these excellent properties, Fe- and Co-based amorphous alloys can be used in different types of sensors. However, the low thermal stability of amorphous alloys has prevented a further extension of application fields. When crystallization occurs, many merits of amorphous alloys are lost.[7] This trend requires a sufficient understanding of crystallization kinetics of amorphous alloys in order to define suitable processing parameters that will yield desirable microstructures and favorable properties.[8] X-ray diffraction (XRD) is one of the most direct methods to study phase transformations. The use of the *in-situ* X-ray opens the possibility for time-resolved kinetic studies. In this article, the crystallization-activation energy and Avrami exponent, *n,* are calculated, and the crystallization mechanisms of the three amorphous alloys are analyzed.

II. EXPERIMENTAL

The master alloy ingots were prepared by melting a mixture of 99.99 pct (with purity) pure elements in an argon atmosphere. Rapidly solidified amorphous ribbons of $Fe_{80}Si_{20}$, $Fe_{78}Si_9B_{13}$, and $Fe_4Co_{67}Mo_{1.5}Si_{16.5}B_{11}$ (in at. pct) with a cross section of 0.02×1.6 mm^2 were prepared in a pure argon atmosphere by the melt-spinning technique. The amorphous nature of ribbon samples was ascertained with XRD measurements processed by a Siemens D5000X diffractometer with the Cu K_α radiation. The sample was heated *in situ* by means of a furnace attached in the diffractometer. This furnace allows sample heating under vacuum conditions (better than 10^{-6} Pa), which prevents sample oxidation during the treatment. The samples were heated at 753 K, 773 K, and 793 K (480 °C, 500 °C, 520 °C, and 550 °C), respectively. After holding these temperatures for 30 and 60 minutes in the furnace, the diffraction data were collected. A parallel experiment was also conducted, using a Nestzsch-STA449C differential scanning calorimeter (DSC) with the same experimental parameters.

III. RESULTS

Figure 1 gives the DSC traces of the $Fe_{80}Si_{20}$ at different heating rates. Taking the heating rate of 10 K/min, for example, two crystallization exothermic peaks

L.J. ZHANG, P.F. YU, and H. CHENG, Ph.D. Candidates, and M.D. ZHANG, D.J. LIU, and Z. ZHOU, Master Students, and Q. JIN and R.P. LIU, Professors, are with the State Key Laboratory of Metastable Materials Science and Technology, Yanshan University, Qinhuangdao 066004, China. P.K. LIAW, Professor, is with the Department of Materials Science and Engineering, The University of Tennessee, Knoxville, TN 37996. G. LI, Professor, is with the State Key Laboratory of Metastable Materials Science and Technology, Yanshan University, and also with the Department of Materials Science and Engineering, The University of Tennessee. Contact email: gli25@utk.edu, gongli@ysu.edu.cn and riping@ysu.edu.cn
Manuscript submitted December 29, 2015.
Article published online October 13, 2016

appear at 817 K (544 °C) and 832 K (559 °C). With increasing heating rate, the peak position shifts to a higher temperature and the peak intensity increases. The exothermic peaks are analyzed by the Kissinger equation, which is described as follows:[9,10]

$$\ln\frac{T^2}{\phi} = \frac{E}{k_B T} + C \qquad [1]$$

where ϕ is the heating rate and k_B is the Boltzmann's constant. The crystallization activation energy, E_{pi}, is deduced from the slope of $\ln(T^2/\phi)$ *vs* $1/T$, where T stands for the peak temperature. By the slope of $\ln(T^2/\phi)$-$1/T$, the crystallization activation energy of the $Fe_{80}Si_{20}$ amorphous alloy can be obtained to be 354.92 and 556.77 kJ/mol, respectively, responding to the first and second crystalline phases. For the other two amorphous samples, the crystallization activation energy can also be obtained by this method. The values of crystallization temperatures and crystallization activation energy of the three samples are listed in Table I.

In order to separate the contributions of the amorphous and crystalline phases during *in-situ* heating samples using the X-ray diffractometer, a fitting procedure of the diffraction peaks was used. Both the first amorphous halo and the (110) diffraction peak of the body-centered-cubic Fe and Si solid solution were fitted, after background subtraction. These results are in good agreement with the data obtained by DSC, assuming that the difference of the exothermic peak areas between annealed samples and as-prepared amorphous alloys is in proportion to the crystallization fraction.[11]

IV. DISCUSSION

DSC curves for $Fe_{80}Si_{20}$, $Fe_{78}Si_9B_{13}$, and $Fe_4Co_{67}Mo_{1.5}Si_{16.5}B_{11}$ amorphous alloy samples annealed at different temperatures and time are displayed in Figures 2, 3, and 4, respectively. Take the DSC tracings of the $Fe_{80}Si_{20}$ amorphous samples, for example: Compared with the as-prepared sample, the DSC curve of the sample annealed at 753 K (480 °C) for 30 minutes still exists in two exothermic peaks, but the intensity obviously decreases, indicating partial crystallization. Both DSC curves of the samples annealed at 753 K (480 °C) for 60 minutes and at 773 K (500 °C) for 30 minutes only have one exothermic peak. When annealed at 773 K (500 °C) for 60 minutes, the exothermic peaks of the sample disappear completely, which indicates

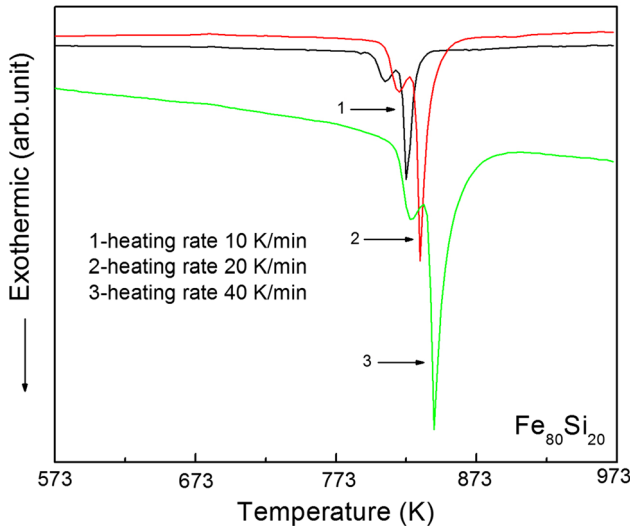

Fig. 1—Peak temperatures obtained from the DSC measurements for the $Fe_{80}Si_{20}$ amorphous alloy as a function of the heating rate.

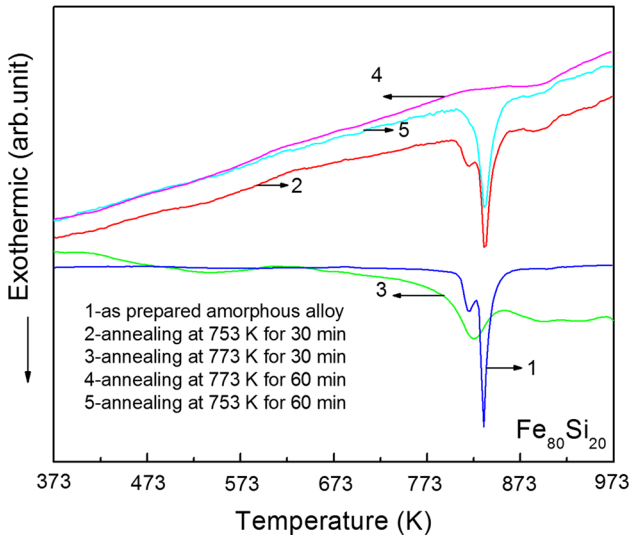

Fig. 2—DSC curves of the $Fe_{80}Si_{20}$ amorphous alloy annealing at different temperatures and times.

Table I. Values of Peak Temperatures and Crystallization Activation Energy of $Fe_{80}Si_{20}$, $Fe_{78}Si_9B_{13}$, and $Fe_4Co_{67}Mo_{1.5}Si_{16.5}B_{11}$ Amorphous Alloys

	$Fe_{80}Si_{20}$ (K/°C)		$Fe_{78}Si_9B_{13}$ (K/°C)		$Fe_4Co_{67}Mo_{1.5}Si1_{6.5}B_{11}$ (K/°C)	
Heating Rate	First Peak	Second Peak	First Peak	Second Peak	First Peak	Second Peak
10 (K/min)	817/544	832/559	815/542	742/469	591/318	853/580
20 (K/min)	825/552	838/565	833/560	860/587	597/324	873/600
40 (K/min)	835/562	850/577	805/532	880/607	600/327	833/560
Crystallization activation energy (KJ/mol)	638/365	830/550	547/274	424/151	476/203	830/557

complete crystallization. The crystallization volume fraction at different annealing temperatures *vs* time can be obtained based on the data in Figures 2 through 4, and shown as in Figure 5.

The time (t) dependence of the crystalline volume fraction (x) was described in terms of the Johnson–Mehl–Avrami equation:[12,13]

$$\ln \ln \frac{1}{1-x} = \ln K_T + n \ln t \qquad [2]$$

where K_T is the reaction speed constant that relates the temperature and phase transition volume fraction x; n is the Avrami exponent, a numerical factor depending on the nucleation and growth processes. The Avrami exponent n can be obtained from the slope of $\ln \ln \frac{1}{1-x}$ *vs* $\ln t$. Here, we transform Figure 5 into $\ln \ln \frac{1}{1-x}$ and $\ln t$ plot (illustrated in Figure 6).[14,15] According to the classical theory, the value of n can describe the crystallization mechanism.[16] The calculated Avrami parameters, which are larger than 2.5 for amorphous alloys, indicate that the crystallization is governed by interface-controlled three-dimensional growth with an increasing nucleation rate.[9,12] In addition, the smaller value of the Avrami parameters than 2.5 for amorphous alloys could be interpreted as the crystallization being governed by diffusion-controlled growth with a decreasing nucleation rate.[14] The n value of 0.87 for the $Fe_4Co_{67}Mo_{1.5}Si_{16.5}B_{11}$ amorphous alloy indicates that when the sample is annealed at 773 K (500 °C), atom diffusion is the main control mechanism in the amorphous-alloy crystallization.[16]

The Avrami exponent n of $Fe_{78}Si_9B_{13}$ annealed at 753 K (480 °C) is 4.12. When $n > 4$, the nucleation frequency increases with the crystallization time, the crystallization is influenced by the interface, and the rate of nucleation accelerates with time. The Avrami

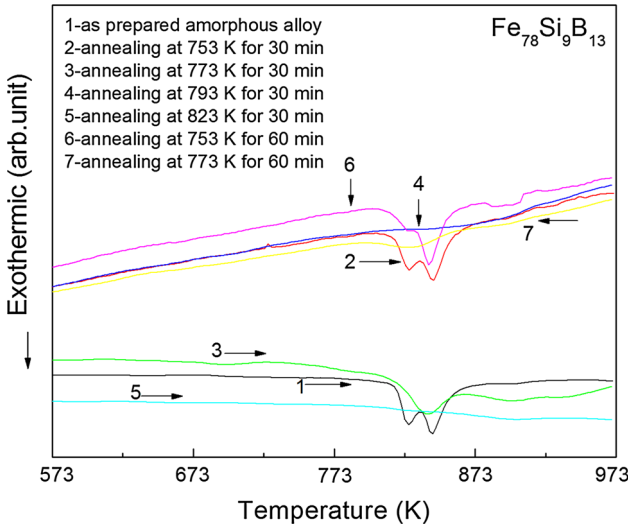

Fig. 3—DSC curves of the $Fe_{78}Si_9B_{13}$ amorphous alloy annealing at different temperatures and times.

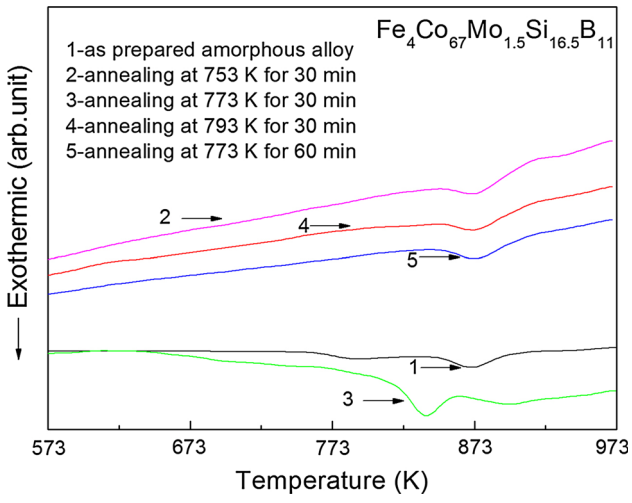

Fig. 4—DSC curves of the $Fe_4Co_{67}Mo_{1.5}Si_{16.5}B_{11}$ amorphous alloy annealing at different temperatures and times.

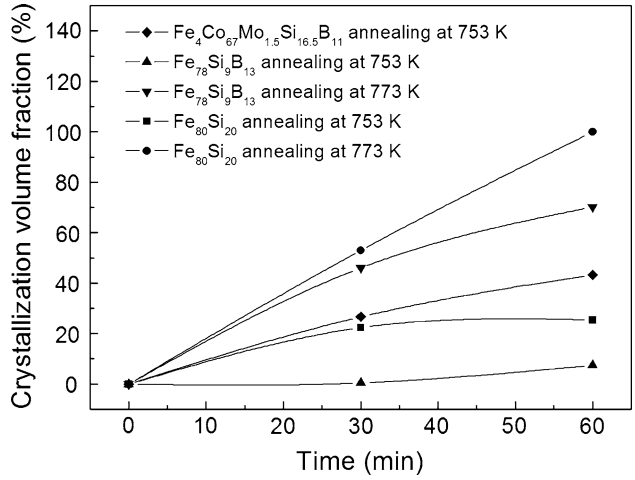

Fig. 5—Relationship between crystallization volume fraction and annealing time.

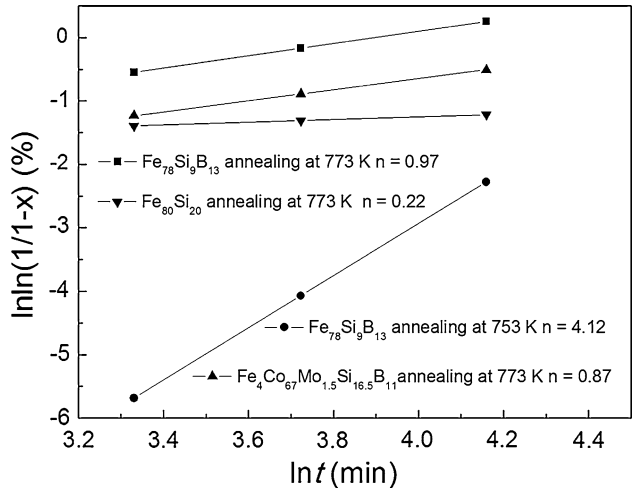

Fig. 6—Johnson–Mehl–Avrami relationship of the three amorphous alloys. The term n is the Avrami exponent.

exponent n of $Fe_{80}Si_{20}$ annealed at 773 K (500 °C) is 0.22, indicating that the crystallization is controlled by diffusion. While annealed at 773 K (500 °C), the Avrami exponents n of $Fe_{78}Si_9B_{13}$ and $Fe_4Co_{67}Mo_{1.5}Si_{16.5}B_{11}$ are 0.97 and 0.87, respectively. The small value of n implies a diffusion-controlled crystallization progress.[17]

V. CONCLUSIONS

The crystallization behaviors of the $Fe_{80}Si_{20}$, $Fe_{78}Si_9B_{13}$ and $Fe_4Co_{67}Mo_{1.5}Si_{16.5}B_{11}$ amorphous-alloys were researched using *in-situ* XRD and DSC at different temperatures and time. The results show that the three amorphous alloys all exhibit two steps of crystallization behavior, the first and second crystallization activation energy for the $Fe_{80}Si_{20}$ amorphous alloy are 354.92 and 556.77 kJ/mol, for $Fe_{78}Si_9B_{13,}$ are 274.23 and 151.82 kJ/mol, for $Fe_4Co_{67}Mo_{1.5}Si_{16.5}B_{11}$, are 202.51 and 136.27 kJ/mol, respectively. When annealed at 773 K (500 °C), the Avrami exponents, $n,$ of the $Fe_{80}Si_{20}$, $Fe_{78}Si_9B_{13,}$ and $Fe_4Co_{67}Mo_{1.5}Si_{16.5}B_{11}$ amorphous alloys are 0.22, 0.97, and 0.87, respectively. The small value of n implies that the crystallization mechanisms of the three amorphous alloys at 773 K (500 °C) are all the diffusion-controlled crystallization progress. While the $Fe_{78}Si_9B_{13}$ amorphous alloy was annealed at 753 K (480 °C), its Avrami exponent, $n,$ is 4.12, which belongs to an interface-controlled crystallization progress.

ACKNOWLEDGMENTS

One of the authors (GL) acknowledges the Specialized Research Fund for the Doctoral Program of Higher Education (Grant No. 20131333110019), the Basic Research Project in Hebei Province (Grant No. A2016203382), and the support from the National Science Foundation of China (Grant No. 11544014). PFY acknowledges the Research Program of the College Science & Technology of Hebei Province (Grant No. QN2016167). PKL acknowledges the Department of Energy, Office of Fossil Energy, National Energy Technology Laboratory (Grant Nos. DE-FE-0008855, DE-FE-0011194, and DE-FE-0024054), Messrs. V. Cedro and R. Dunst, program managers. PKL is also grateful for the support from Project No. DE-FE-0011194, Dr. J. Mullen, project manager; the U.S. Army Research Office (Project No. W911NF-13-1-0438), Dr. D.M. Stepp, program manager; and the National Science Foundation (Grant No. CMMI-1100080), Dr. C. Cooper, program director. TE was supported by the Department of Energy, Office of Sciences, Basic Energy Sciences, Materials Science and Engineering Division.

REFERENCES

1. A. Inoue, F.L. Kong, Q.K. Man, B.L. Shen, R.W. Li, and F. Al-Marzouki: *J. Alloys Compd.*, 2014, vol. 615, pp. S2–S8.
2. W. Gerhard: *J. Non Cryst. Solids*, 2002, vol. 307, pp. 853–62.
3. A. Inoue and J.S. Gook: *Mater. Trans. JIM*, 1995, vol. 36, pp. 1180–83.
4. A. Inoue, H.K. Oshiba, T. Zhang, and A. Makimo: *J. Appl. Phys.*, 1998, vol. 83, pp. 1967–74.
5. F.L. Kong, C.T. Chang, A. Inoue, E. Shalaan, and F. Al-Marzouki: *J. Alloys Compd.*, 2014, vol. 615, pp. 163–66.
6. A. Inoue, B.L. Shen, and C.T. Chang: *Intermetallics*, 2006, vol. 14, pp. 936–44.
7. W.H. Wang, C. Dong, and C.H. Shek: *Mater. Sci. Eng. R*, 2004, vol. 44, pp. 45–89.
8. Z.P. Lu, C.T. Liu, JR Thompson, and W.D. Porter: *Phys. Rev. Lett.*, 2004, vol. 92, pp. 245503/1–245503/4.
9. X. Li, Z. Cheng, K. Hu, H. Chen, and C. Yang: *Vacuum*, 2015, vol. 114, pp. 93–100.
10. N. Bayri, V.S. Kolat, T. Izgi, S. Atalay, H. Gencer, and P. Sovak: *Acta Phys. Pol. A*, 2016, vol. 129, pp. 84–87.
11. H.S. Chen: *J. Non Cryst. Solids*, 1978, vol. 27, pp. 257–63.
12. X. Wang, D. Wang, B. Zhu, Y. Li, and F. Han: *J. Non Cryst. Solids*, 2014, vol. 384, pp. 111–16.
13. H.Y. Jung, M. Stoica, S. Yi, D.H. Kim, and J. Eckert: *Metall. Mater. Trans. A*, 2015, vol. 46 (6), pp. 2415–21.
14. Y.D. Sun, P. Shen, Z.Q. Li, J.S. Liu, M.Q. Cong, and M. Jiang: *J. Non Cryst. Solids*, 2012, vol. 358, pp. 1120–27.
15. S.M. Kim, D. Chandra, N.K. Pal, M.D. Dolan, W.M. Chien, A. Talekar, J. Lamb, S.N. Paglieri, and T.B. Flanagan: *Int. J. Hydrog. Energy*, 2012, vol. 37, pp. 3904–13.
16. D. Turnbull: in *Solid State Physics,* F. Seitz and D. Turnbull, eds., Academic Press, New York, NY, 1956, vol. 3, pp. 225–306.
17. J.W. Christian: *The Theory of Transformation in Metals and Alloys*, 2nd ed., Pergamon Press, Oxford, 1975.